On the role of the spherulitic microstructure in fatigue damage of pure polymer and glass-fiber reinforced semi-crystalline polyamide 6.6

I. Raphael[a,b,*], N. Saintier[a,*], G. Robert[b], J. Béga[a], L. Laiarinandrasana[c]

[a] I2M, Arts et Métiers ParisTech, Esplanade des Arts et Métiers, 33405 Talence, France
[b] Solvay Performance Polyamides, Avenue Ramboz, BP 64, 69192 Saint-Fons, France
[c] PSL Research University, MINES ParisTech, Centre des Matériaux, CNRS UMR 7633, BP 87, 91003 Evry, France

ARTICLE INFO

Keywords:
Fatigue damage
Composite material
Semi-crystalline polymer
Oriented spherulites

ABSTRACT

Understanding fatigue damage mechanisms in short fiber reinforced thermoplastics is a key issue in order to optimize material processing and propose physically based multiscale fatigue damage models. The present work aims at further understanding observations of fatigue damage in the polyamide 6.6 matrix with respect to its semi-crystalline structure. In this paper the polymer and associated composite are tested in their ductile regime i.e. above the glass transition temperature. Tomographic and SEM observations are used in order to establish a damage scenario at the spherulitic scale. These observations prove that fatigue damage progresses by intra-spherulitic failure in their equatorial plane. Observations of the spherulite nuclei also evidence the oriented structure of the semi-crystalline polymer induced by the injection-molding manufacturing process.

1. Introduction

In order to comply with regulations, automotive manufacturers are increasingly using composite materials to engineer lighter cars. Short glass fiber reinforced (SFRP) polyamide 6,6 (PA66) is used in multiple applications, including key components in the case of the car industry. Getting a good grasp of the damage mechanisms under fatigue loading condition is thus a crucial research aspect. Better understanding damage processes will lead to better fatigue damage models and help engineers to design materials and parts more efficiently.

Multiple works have contributed to establish damage scenarios for the composite material, using fractography observations [1–3] and, more recently, tomographic data [4,5]. Saintier et al. [6–8] have shown the particular importance of understanding matrix damage to fully understand the overall composite fatigue damage scenario, as cavitation and crazing in the thermoplastic matrix appear to be precursors of all other fatigue damage process in SFRP materials. In particular, it was shown that short fatigue cracks in SFRP propagate with a characteristic length of about 25 μm in well defined steps. Once segmented on tomographic data they appear as flat penny-shaped structures with a diameter close the spherulite size [6] and proposing a strong interaction between fatigue damage localization and the polymer microstructure. Hypothesis was thus made that fatigue damage in the matrix is intra-spherulitic and that cracks advance by opening spherulites in their equatorial planes, this spherulite opening being triggered by cavitation.

The role of the spherulitic structure on damage development of PA6 matrix was already observed during simple tensile and creep loading by two studies. Galeski et al. [9] analyzed spherulitic damage in bulk PA6 during quasi-static tensile testing. They noted that “equatorial regions of the spherulites are particularly susceptible to microvoiding mechanisms”. More recently, Selles et al. [10] studied the influence of the spherulitic structure on the damage mechanisms for the creep failure of PA6. They showed extensive damage taking place both in the polar regions of the spherulites and in the equatorial plane. Similar analysis of the link between bulk damage and the semi-crystalline structure of the polymer was needed for fatigue loading.

The above mentioned scenario for fatigue loading is supported by two previous works on fatigue damage. The first one concerns the earlier work of Bretz [11,12] who suggested that semi-crystalline polymers fracture both in an inter-spherulitic and an intra-spherulitic manner (also called *trans-spherulitic* by the authors). The authors performed uniaxial fatigue testing at 10 Hz, but precise loading conditions are unclear. The quality of the images is lacking of sufficient details to make firm conclusion and, as noted by the authors themselves, more work is needed in this area [12]. The second one relates to the work of Mourglia-Seignobos [13], based on SAX measurements, that reported the fatigue damage to occur in domains oriented perpendicularly to the stress. This damage being *very likely* located in the equatorial plane of spherulites, between crystalline lamellae.

However in order to validate such a scenario, further understanding

* Correponding authors.
E-mail addresses: ilan.raphael@ensam.eu (I. Raphael), nicolas.saintier@ensam.eu (N. Saintier).

https://doi.org/10.1016/j.ijfatigue.2019.04.036
Received 12 February 2019; Received in revised form 23 April 2019; Accepted 26 April 2019

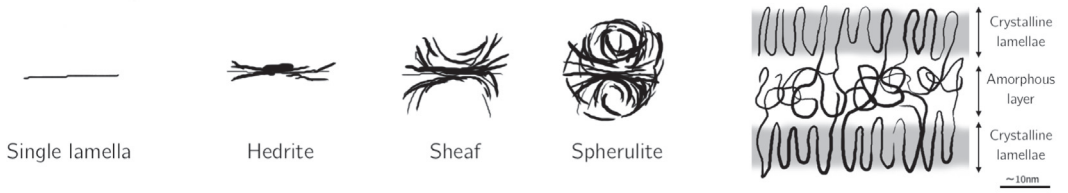

(a) Formation of a spherulite in a thin film

(b) Semi-crystalline arrangement of polymer chains

Fig. 1. Formation and structure of spherulites in a semi-crystalline thermoplastic.

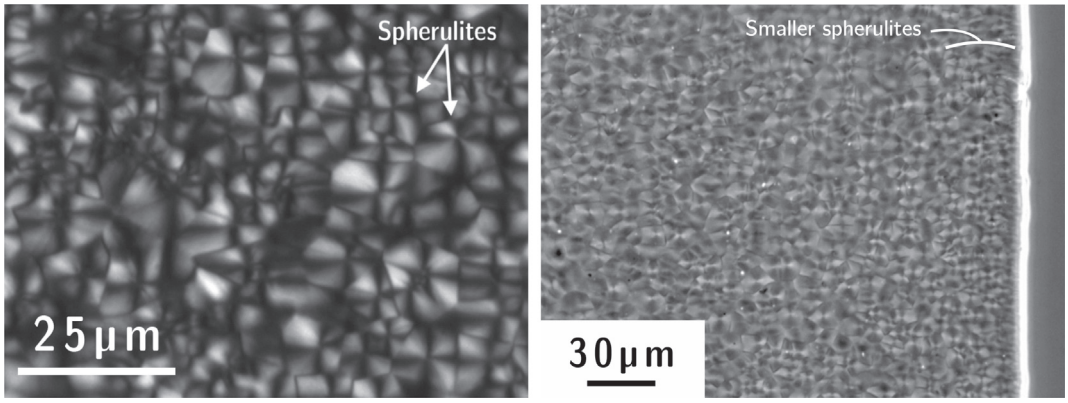

(a) Core of the specimen

(b) Surface of the specimen

Fig. 2. Spherulites in PA66 observed using polarized light microscopy on thin slices obtained by microtomy.

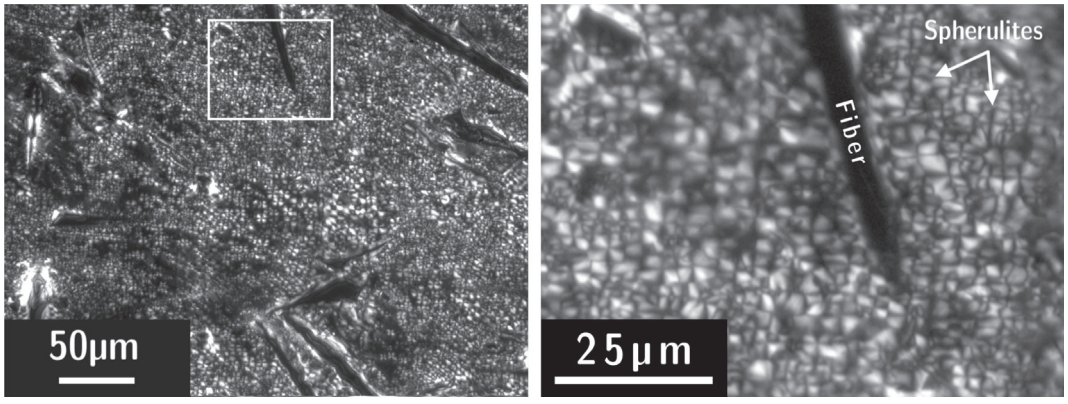

(a) General view

(b) Detail at fiber tip

Fig. 3. Spherulites observed using polarized light microscopy on thin slices of reinforced PA66 obtained by microtomy. Slicing was performed in a longitudinal direction compared to fibers, which gives better view of the microstrucutre but is more challenging than transversal cut as usually performed for bulk composite material [6,13].

and observations evidencing this spherulitic fatigue damage are required. This paper aims at further analyzing the link between the spherulitic microstructure and fatigue damage.

2. Material and methods

2.1. Spherulites

Semi-crystalline thermoplastics often crystallize as spherulites, usually distributed as spherical crystal colonies. Their formation is generally described during crystallization experiments on thin films [14]. In this case, each spherulite forms from a single lamella - the "nucleus" of the future spherulite. These prespherulitic structures are randomly oriented [15]. Further crystallization make them grow into a hedrite, a sheaf and later a full spherulite (Fig. 1(a)) [16]. Multiple mechanisms have been put forth to explain the formation of such spherulite from a single lamella. These scenarios -as well as much more detailed information- can be found in the review by Crist and Schultz [17]. However experimental evidence on the mechanisms of spherulite growth in the bulk material is, understandably, lacking. Knowledge of the three-dimensional structure of spherulites is thus largely incomplete.

In the case of the polymer studied and process conditions, spherulites are considered to be composed of an array of crystalline lamellae between which the polymer is in an amorphous state (Fig. 1(b)). Lamella thickness is around 10 nm, as is the distance between to successive lamellae.

Spherulite growth continues linearly with time until it encounters neighboring growing spherulites. The average size of the spherulites depends upon the cooling conditions and the density of potential nucleating sites for crystallization.

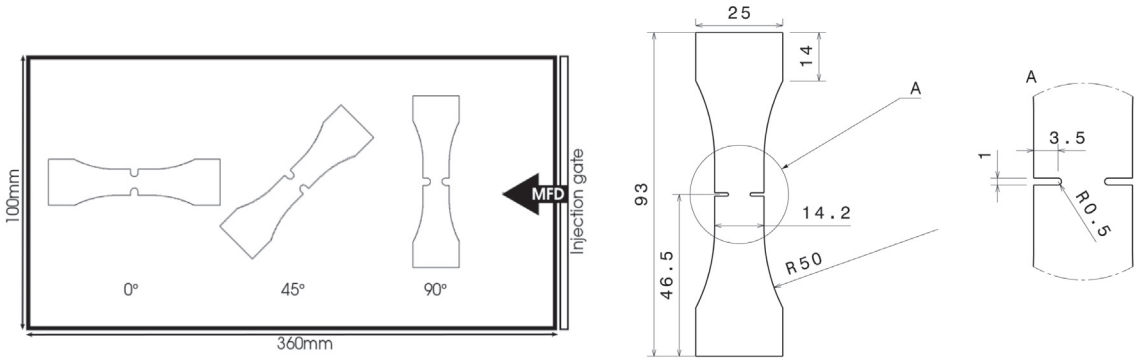

(a) Specimen orientation

(b) U0.5 notched geometry

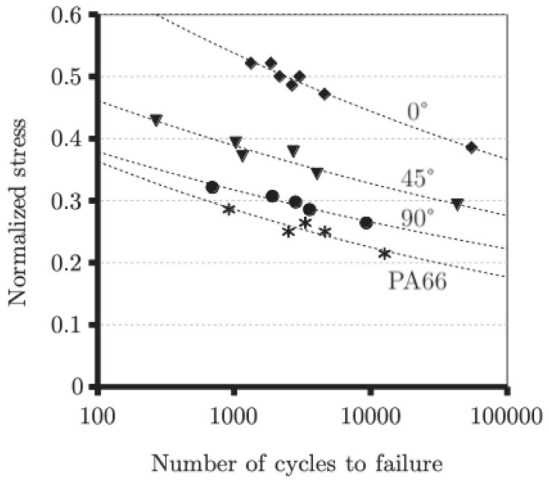

(c) Normalized S-N curves

Fig. 4. Geometries and S-N curves for the notched specimens.

Table 1
Parameters for the different fatigue specimens. σ_{max} is the maximal nominal stress. N_f stands for the number of loading cycles prior to failure. Interrupted specimens are marked as "int." with the corresponding number of cycles.

Material	Notch	σ_{max} (MPa)	N_f
PA66 "90°"	U0.5	40	917
PA66 "90°"	U0.5	30	12656
PA66 "0°"	U0.5	45	1858
PA66 "45°"	U0.5	45	1835
PA66GF30 90°	U0.5	57	1241
PA66 "90°" + cryofrac.	U0.5	35	int. 2531 (95%N_f)
PA66 "90°" + cryofrac.	U0.5	38	int. 4221 (90%N_f)
PA66GF30 45°	N/A	62	int. 1500 (98%N_f)

2.2. Observation of spherulites

Detailed observation of spherulites is crucial if one wants to link the fatigue damage to the spherulitic structure of the polymer. However, unlike with grains observations in metals where crystallographic observations can be made using EBSD and grain boundaries can be observed in tomography by various techniques [18], observation of spherulites is much less standardized. Multiple observation techniques can be found in the literature [17], but the full understanding of the complex tridimensional nature of bulk polymer's spherulite is still an issue.

Traditional observations are made using polarized light microscopy (see Figs. 2 and 3). Thanks to the birefringence of the material, spherulites appear with a typical Maltese-Cross pattern [19,20]. Such methods require the observation to be made on thin film (obtained by casting or cut from samples using a microtome), making it delicate for a number of applications. In particular the observation of damage by this technique is difficult and may lead to ambiguous conclusions. It is also worth mentioning that obtaining longitudinal thin slices of the fiber reinforced material using a microtome is possible but arduous. The polymer around the fibers is damaged by the process and it is difficult to observe the spherulites in these regions. Moreover, as it is based on optical microscopy, this technique is better suited for large spherulites.

Observations of spherulites and damage can also be made using Atomic Force Microscopy (AFM) [21,22]. Once again, published observations have mostly been performed on thin films, yielding the same aforementioned limitations.

Finally, cryo-fractography and/or chemical etching have also successfully been used in some studies [23,24] and especially for PA6 [25,10], for PEHD [26,27] and for PA11 [28]. However they are not easily implemented and chemical attacks to reveal spherulites can be very tricky to manage. This might explain the very few (convincing) examples that can be found in the literature.

It is worth noting that spherulites in PA6 and PA66 are not visible using tomography [6,10] - at least with the technology currently available, although new techniques are currently under development using nano-tomography. For these reasons, initial microstructures will be evaluated from polarized observations of microtome slices (2 µm thick) obtained from the bulk polymer and composite. Damage

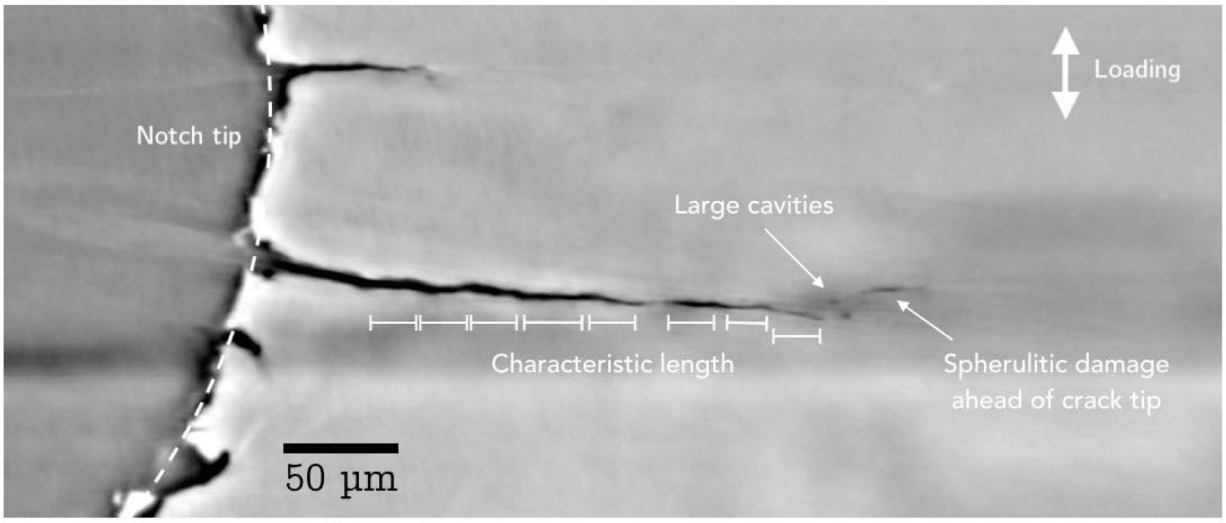

(a) 2D slice

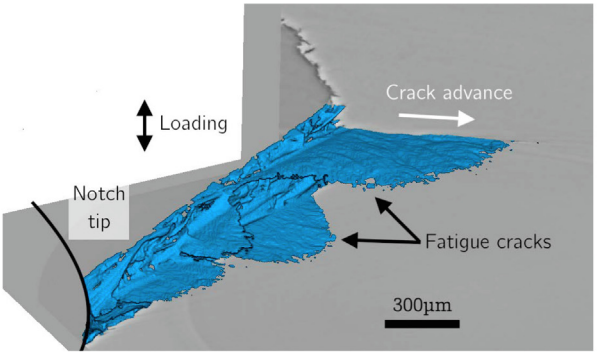

(b) Segmented view of the fatigue cracks

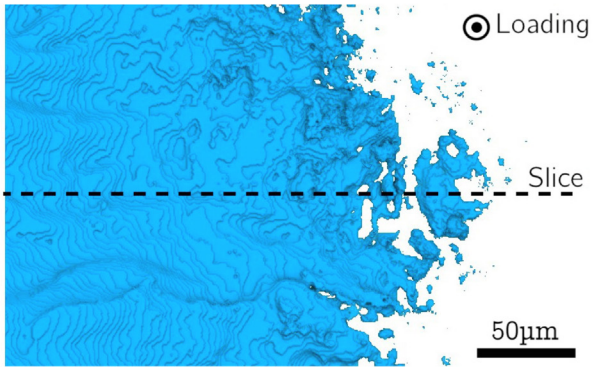

(c) Detailed top view of the segmented crack tip and position of the 2D slice from fig. 5(a)

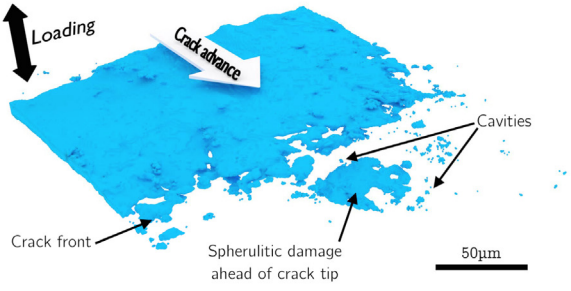

(d) Segmented view of the crack tip

Fig. 5. Tomographic observation and segmentation of the crack tip in a PA66 notched specimen, test interrupted at 4221 cycles and 90% of estimated fatigue life.

evaluation will be assessed from tomographic observations combined to fractographic Scanning Electron Microscopy (SEM) analysis. Surface metallization was necessary, the samples were thus coated by a nanometric layer of Au by sputter deposition. Observations were performed using a Zeiss Evo15 HD SEM.

2.3. Material

Both unreinforced and reinforced PA66 were studied in this work. These materials are supplied by Solvay Performance Polyamides.

The study of the unreinforced material made observation of the spherulitic damage mechanisms easier, as spherulitic structures have a size comparable to the fiber diameter. The transposition of the damage scenario established in unreinforced material to the case of matrix in the composite material is verified by experimental observations presented at the end of this work.

2.3.1. Pure PA66

Fig. 2(a) illustrates the microstructure of the pure PA66 as observed by polarized light microscopy. Spherulites diameters are in the range of 15–30 µm. However this size varies throughout the thickness of the specimen, especially on a 30 µm distance from the surface of the specimen where spherulites are notably smaller (Fig. 2(b)).

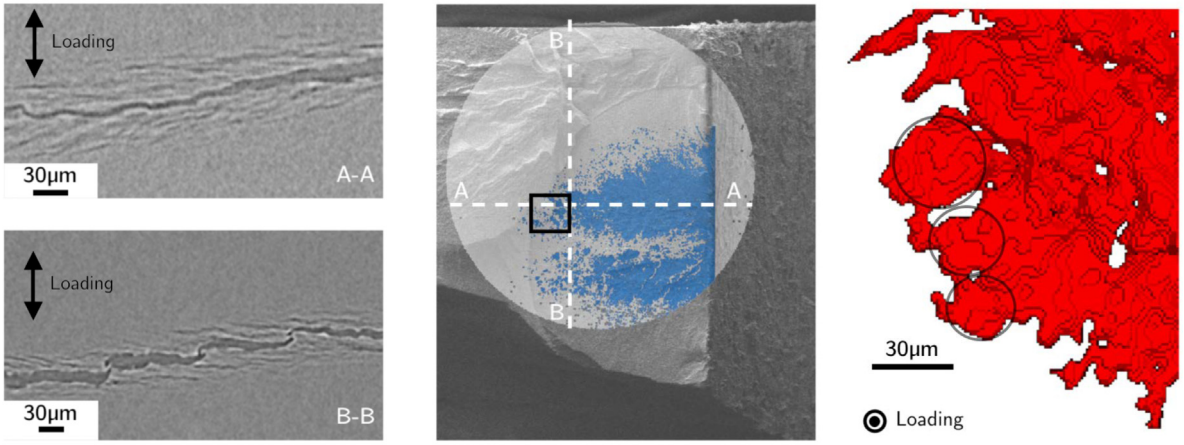

(a) 2D views (black squared area in figure 6(b))

(b) Fracture surface with the segmented crack ovelayed

(c) Detailed view of the segmented crack tip (black squared area in figure 6(b))

Fig. 6. Crack tip in a PA66 notched specimen as observed by microtomography, test interrupted at 2531 cycles and 95% of estimated fatigue life.

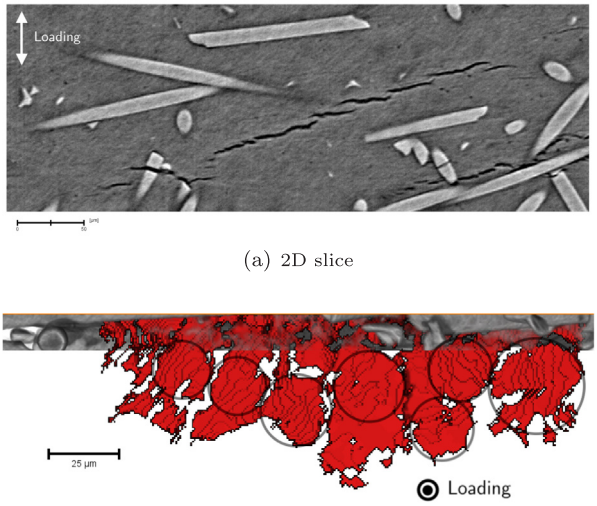

(a) 2D slice

(b) 3D view of the segmented damage

Fig. 7. Short cracks in a reinforced 45° PA66 smooth specimen as observed by microtomography, test interrupted at 1500 cycles and 98% of estimated fatigue life.

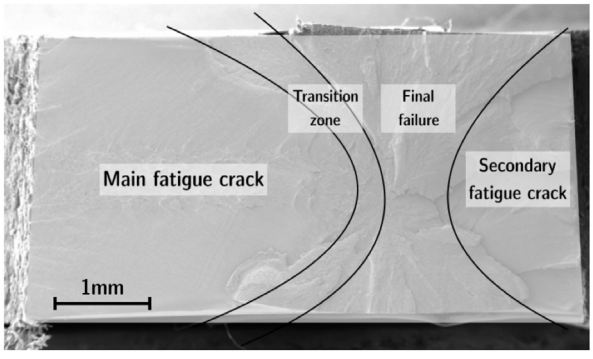

Fig. 8. Fracture surface of a notched PA66 specimen after fatigue testing (N_f = 917).

2.3.2. Short glass fiber reinforced PA66

The commercial grade of PA66 reinforced by 30 wt% of short glass fibers is a Technyl® A218V30. Injection molding induces a characteristic microstructure in the composite: fibers orientation is heterogenous throughout the thickness of the plate. This microstructure has been extensively described in the literature and is usually referred to as a *skin-shell-core* microstructure.

The reader shall refer to the articles written by the following authors for more details regarding fiber orientation in injection molded composite materials: Horst [2], Bernasconi [29], Arif [4,8], Ayadi [30] and Rolland [7].

Fig. 3 illustrates the microstructure in the composite material. These observations clearly indicate that the spherulite size depends on the local microstructure. Close to the fibers, spherulites are smaller and harder to observe. In poorly reinforced areas, although a bit smaller, spherulite morphology is similar to the one observed in pure PA66. This smaller spherulite size can be explained by the increased number of sites for potential nucleation on the surface of fibers or fiber glass *dust* resulting from the manufacturing process, and heterogenous cooling rates at the microstructural level.

2.4. Specimens geometry and loading conditions

Fatigue specimens are waterjet-cut from injection-molded rectangular plates 3.24 mm thick. Samples can be cut from plates along three directions with respect to the MFD: 0°, 45° and 90°(Fig. 4(a)) for both pure and reinforced polymer. Specimens are designated by the direction of their main axis with respect to the MFD. The use of notched specimens allows for the localisation of the damage to make the observation of fatigue damage by tomography easier. The notched geometry that was considered here is a symmetric “U” notch of 0.5 mm in radius (Fig. 4(b)).

Finally, as mechanical behavior and fatigue damage of PA66 is humidity dependent, all specimens were conditioned at a relative humidity (RH) of 50% and 23° C for two weeks prior to testing and experiments were also conducted at 23° C. For these conditions, the polymer and associated composite are tested in their ductile regime i.e. above the glass transition temperature. Fatigue tests were performed under load control on a Bose Fatigue machine (electromagnetic fatigue machine that does not induce external heating on the specimen due to its “cold” technology), at a loading ratio of R = 0.1 and a frequency of 0.5 Hz (a sufficiently low frequency to ensure a low heat build-up during fatigue tests).

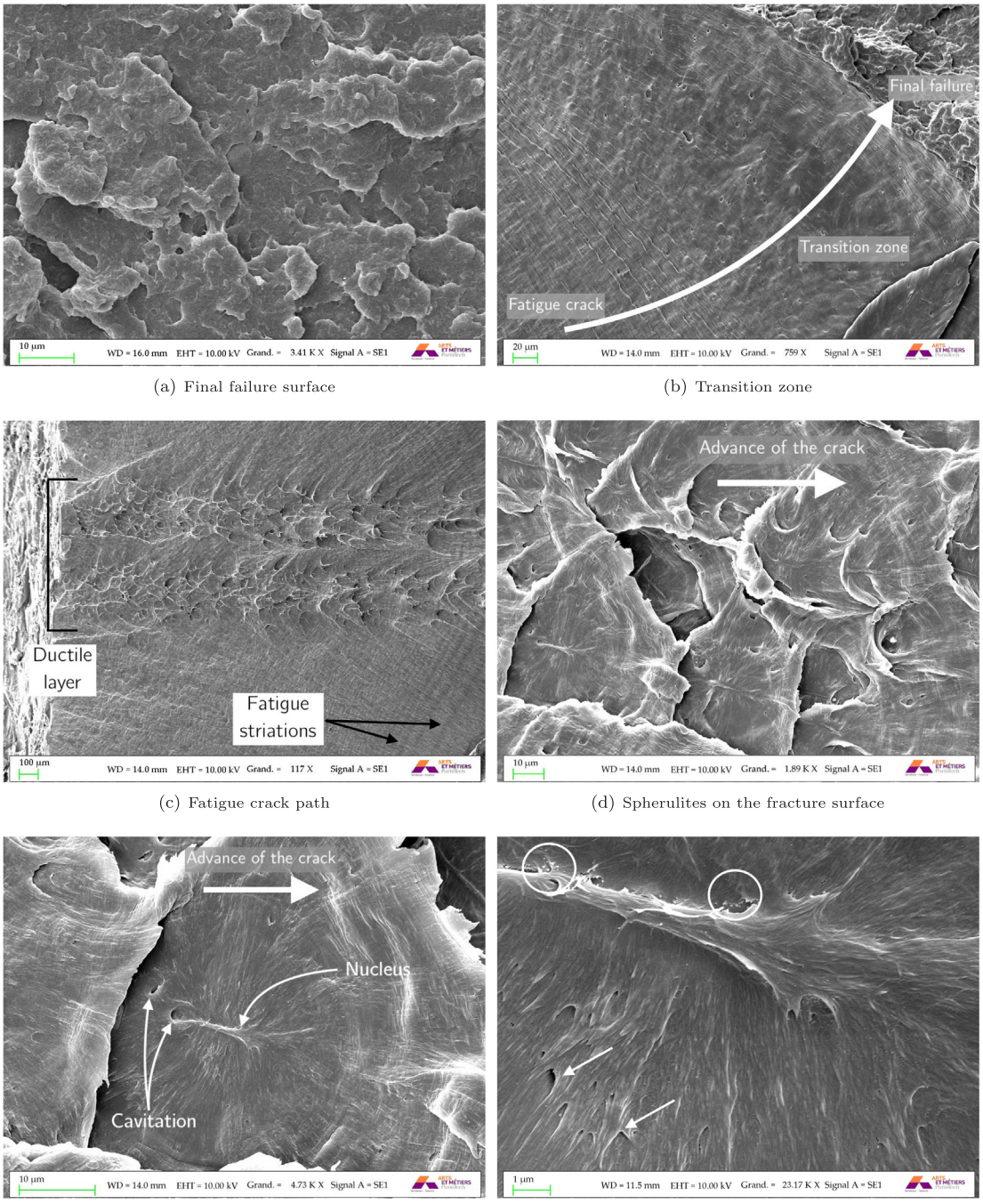

(a) Final failure surface

(b) Transition zone

(c) Fatigue crack path

(d) Spherulites on the fracture surface

(e) Detail of a spherulite

(f) Detail of the nucleus from fig. 9(e)

Fig. 9. SEM fractography of a notched PA66 specimen (N_f = 917).

2.5. Tomographic observations

Synchrotron X-ray tomography was used in order to investigate bulk damage in the specimens. Acquisition was performed on the Psyché beamline at the SOLEIL synchrotron. The filtered X-ray beam (2 mrad mirror, 0.5 mm aluminum and 0.25 mm silver) had an energy of about 26 keV. The CMOS detector with 6.5 μm pixels, was associated to a × 10 objective, leading to a voxel edge size of 0.65 μm on the acquired image (for more details see [6]). This allowed for the high image resolution necessary to observe the early stages of damage.

Data analysis and segmentation was performed using the Avizo commercial software. Choose of the thresholds for visualization was based on the experience in small-crack and cavitation segmentation from previous works [6].

3. Results and analysis

A full data base was constructed including RH and loading ratio effects. However the focus of this paper being to identify fatigue damage mechanisms only a few tests results are given here. Two types of fatigue tests were performed. First, interrupted fatigue tests so that very short fatigue cracks could be initiated in the pure PA66 specimens and in the reinforced polymer for tomographic observations of the very first stages of damage. In addition two tests were interrupted, scanned by tomography then cryo-fractured in order to freeze the damage situation at the crack tip, locate possible damage markers and compare to the

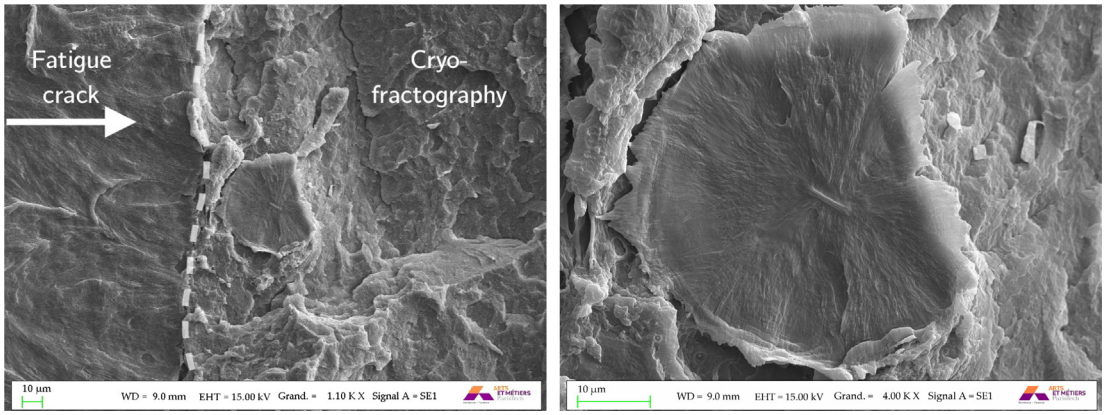

(a) Limit between fatigue crack and cryofractography (b) Top view of the spherulite

Fig. 10. Spherulitic damage ahead of the fatigue crack in a notched PA66 specimen after cryofractography, test interrupted at 4221 cycles and 90% of estimated fatigue life.

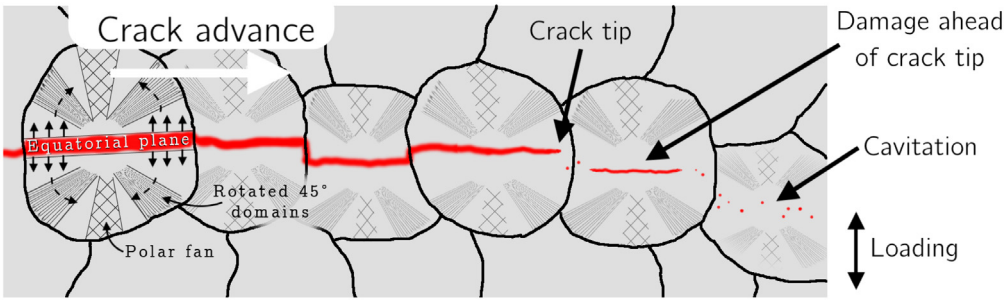

(a) Side view of the crack advance

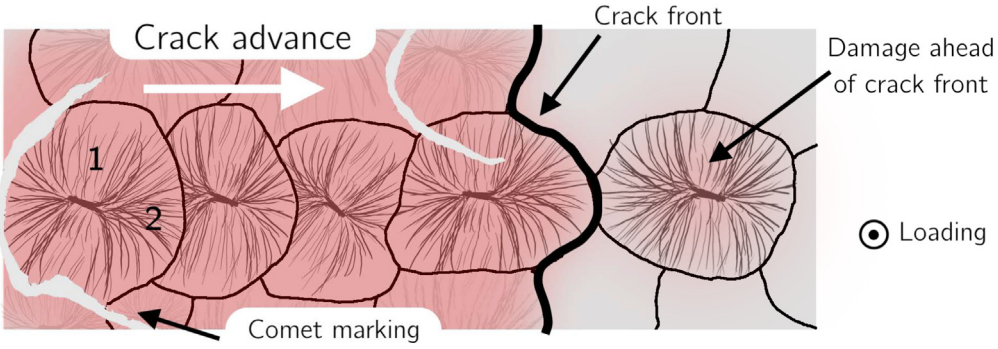

(b) Top view of the crack advance

Fig. 11. Schematic of the influence of the spherulitic structure of the polymer on fatigue crack advance.

tomography observations. Second, additional tests were performed up to failure to analyse the fracture surface. The loading parameters for the different specimens for which observations are given in this paper are listed in Table 1 and normalized S-N curves are given on Fig. 4(c). The stress indicated as σ_{max} is the maximal nominal engineering stress imposed during cyclic loading in the net section of the specimen (area between the two notches).

3.1. Tomographic observations on short fatigue cracks

Interrupted fatigue specimens were observed using tomography after the initiation of a mesoscopic crack (a few millimeters in size). Typical examples of fatigue cracks as observed on pure PA66 are given on Fig. 5 for a several millimeters crack and on Fig. 6(b) for what can be considered as a short fatigue crack (few hundred microns in length).

Fig. 5(a) and (b) represent respectively the 2D view and segmented view of the fatigue crack initiation. Several short fatigue cracks can be identified at the notch indicating simultaneous initiation at different locations in the notch area. Once initiated from the notch root, fatigue crack then propagates with a slightly irregular trajectory, as observed on Fig. 5(a). By close examination of tomographic slices (tens of slices have been analyzed to come up to that conclusion even if only one is given here), it is possible to identify a characteristic length of 20–30µm along the crack propagation direction. In addition, these observations evidence the presence of damage ahead the crack tip.

Indeed, both small cavities of a few microns and micro-cracks can clearly be observed ahead the crack tip. It is worth noticing that the characteristic size of the micro-crack and of the crack propagation pattern is of the order of magnitude of the spherulites. These observations confirm also that cavitation very near the crack tip seems to play a

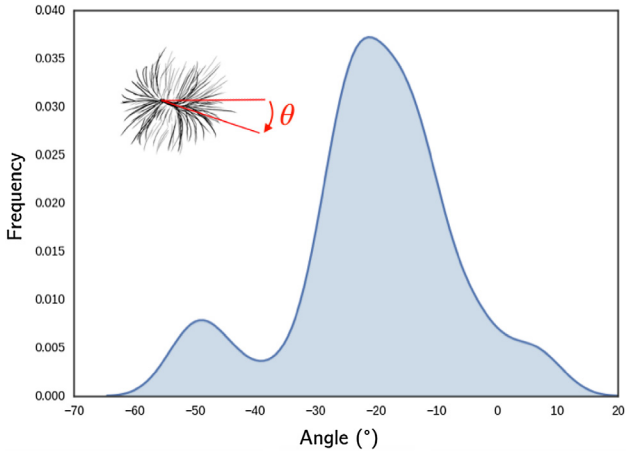

Fig. 12. Orientation of the 40 nuclei observed on 3 different PA66 specimens after fatigue testing.

major role in the fatigue crack propagation process.

Fig. 5(c) and (d) give additional information on these damage precursors. First, the top view of crack front indicates a very irregular crack front with significant diffuse damage ahead of the crack front. Considering the size (in the micrometer range) and aspect ratio of these damage markers they most probably correspond to the cavitation process identified on Fig. 5(a). In addition to this cavitation process, some larger damaged area can be clearly identified. Once segmented, they appear as flat, penny shape like volumes about 20 μm in diameter (see Fig. 6(c)). This size and shape strongly suggest that these penny shaped damage zones correspond to intraspherulitic damage developing ahead the crack tip.

In the case of reinforced polymer, an example of fatigue microcracks is given Fig. 7(b). The top view clearly confirms the presence of a multiplicity of penny shape damaged zones that combined constitute the short fatigue crack. These observations appear very similar to the one observed on pure PA66 so that the same mechanisms are proposed for both reinforced and un-reinforced polymer.

Based on these observations a scenario has been proposed in which the damage is localized in the equatorial plane of the spherulites and the crazing structures observed by tomography can be associated to an intra-spherulitic fatigue crack propagation process in the equatorial plane, resulting in spherulites being *cut in half*.

However, because spherulites in PA66 are not visible using tomography, these observations and damage scenario need to be completed by other observation techniques in order to confirm the nature of the spherulitic damage.

3.2. Fractography analysis of fatigued PA66 specimens

3.2.1. Spherulite observations

The idea behind the observations presented hereafter is that if the fatigue crack results from the opening of the spherulites in their equatorial planes, half of the spherulite should be observable on the fracture surface. A somewhat analogous image (but less precise) can be found in the literature, where the spherulite can be distinguished [12].

Fracture surfaces obtained after fatigue loading on notched PA66 specimens can be divided into several regions: the main and secondary fatigue crack area starting from the notches on both sides, the final failure surface and a transition zone in between the two (Fig. 8).

The final failure surface, at the center of the specimen, exhibits a patchy irregular surface (Fig. 9(a)). Some authors suggested that the patches are related to the spherulites [12], although possible, this seems far from being evident just by looking at the fracture surface.

The transition zone, between the fatigue crack path and the final fracture surface, is rather smooth. An important number of cavities can be observed in this region (Fig. 9(b)).

In the fatigue crack paths on both sides, one can observe parabolic fatigue striations on the outer layers of the specimen (Fig. 9(c)). On the center, a layer of rough aspect can be observed compared to the surrounding matrix. This rough layer could be explained by greater strain levels at the center of the specimen or, although less likely based on our observations (Fig. 2), by a gradient in the material properties [31]. By taking a closer look in this region, we can unambiguously observe the spherulites (Fig. 9(d) and (e)). Fracture surface roughness appears to be induced by the interaction of the crack with the spherulitic microstructure and clearly indicate that the crack has followed the equatorial planes of the different spherulites on its path.

Observations of a specimen submitted to interrupted fatigue loading followed by cryofractography in traction help further explicit the damage scenario. Fig. 10 illustrates the spherulite damage ahead the crack tip. At the time where cryofractography was performed, the spherulite was already damaged by the fatigue loading. This observation, together with Fig. 5(a), definitively confirm that spherulitic damage occurs ahead of the main fatigue crack front.

Furthermore, as the nuclei of the spherulites can be seen on the fatigue fracture surface of the different specimens, this confirms the scenario of an intra-spherulitic failure in the equatorial plane. The nucleus seems harder and denser than the surrounding lamellae and may act as damage precursor. Small cavities that can be found close to the nucleus (Fig. 9(f)) confirm this point as well as small white spheres that could be nucleating agents introduced during the manufacturing process.

The 2D tomographic observations of a characteristic damage length and the 3D observations of disk-like structures allow to propose a

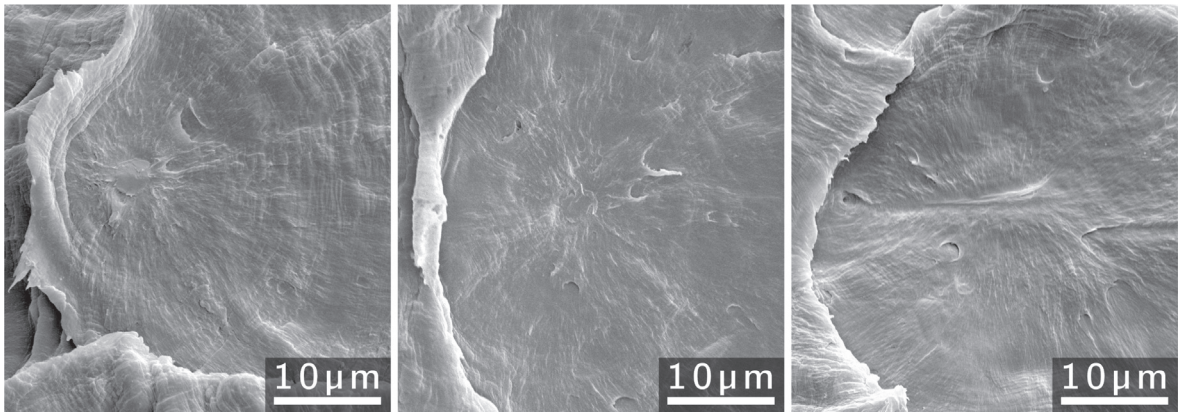

(a) 0° specimen (b) 45° specimen (c) 90° specimen

Fig. 13. SEM observations of the nuclei for three different specimens orientation ($N_f \approx 1500$).

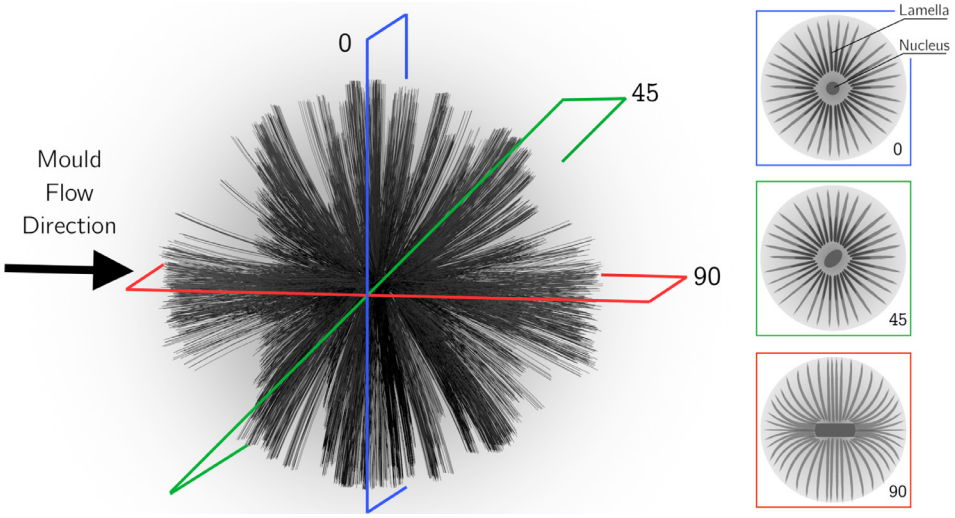

Fig. 14. Oriented spherulitic structure induced by the injection molding.

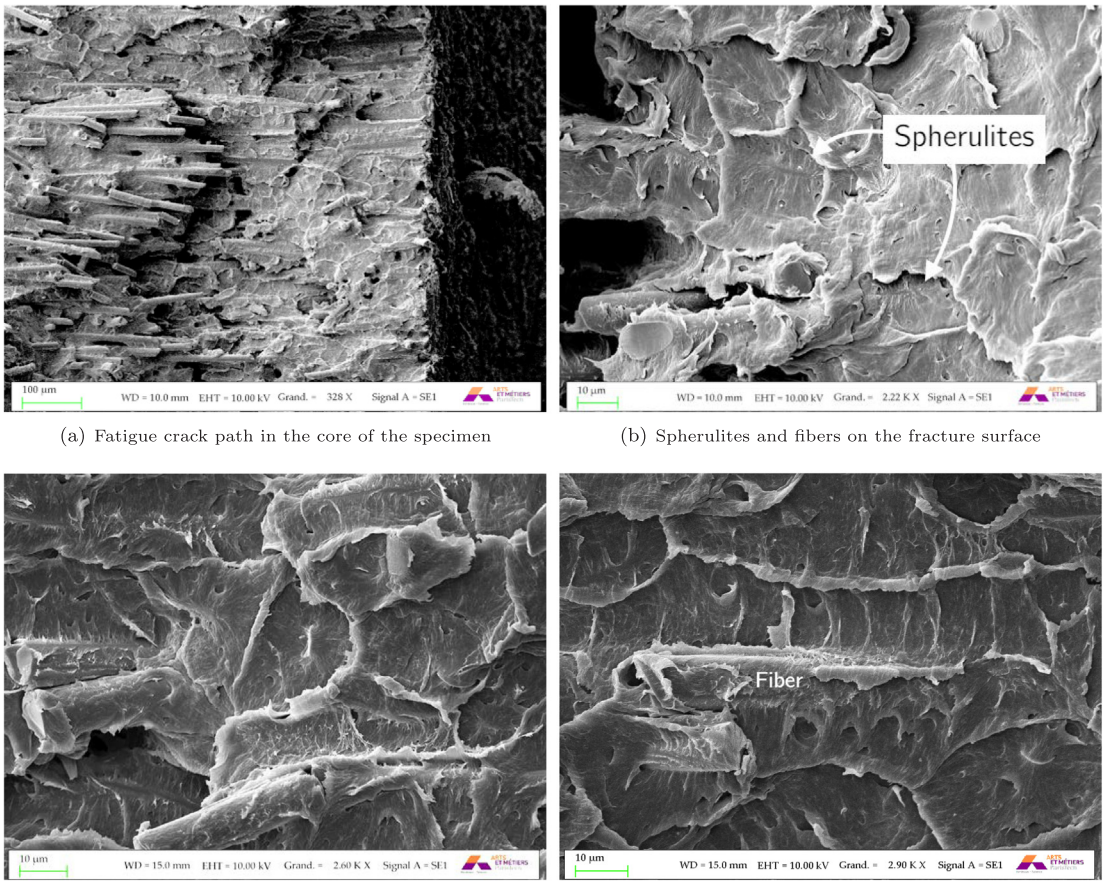

(a) Fatigue crack path in the core of the specimen

(b) Spherulites and fibers on the fracture surface

(c) Spherulites and fibers on the fracture surface

(d) Spherulites along a fiber

Fig. 15. SEM fractography a notched reinforced PA66 (fibers at 90° in the core, $N_f = 1241$).

damage propagation scenario as illustrated Fig. 11. Locally, the crack takes a path that depends on the spatial spherulitic arrangement.

It can be noted that the crack propagates either perpendicularly (region 1 on Fig. 11(b)) or parallel (region 2 on Fig. 11(b)) to the lamellae in the equatorial plane. More diffuse damage might also develop in other regions of the spherulite (see Fig. 11(a)) for longer cracks, as suggested by Fig. 6(a). However more precise tomographic (nano-tomography) data would be required to fully assess the nature of this secondary damage.

Finally it is worth mentioning that equatorial damage processes were already observed using SEM by Ben Hadj Hamouda for creep fracture of a medium density ethylene-butene copolymer [26], suggesting some similarities between fatigue and creep damage. These aspects will be further discussed in a forthcoming paper.

3.2.2. *Spherulite orientation*

The orientation of the nuclei with respect to the horizontal can be measured on the images (Fig. 12). As they seem to be preferentially

oriented in a given direction, it is likely that the orientation of the nuclei is induced by the injection process. All nuclei would then be aligned because the specimens were all cut at 90° with respect to the MFD.

Pure PA66 samples were thus cut at 0° and 45° for further analysis. After fatigue loading and observation of the fracture surface, the nucleus clearly appears as a disc on the fracture surface of 0° specimens (Fig. 13(a)). For 45° specimens the nucleus can have a slightly elliptical shape, although being harder to observe (Fig. 13(b)). Conversely, for the 90° specimen, the nucleus appears as a *rectangle* with high aspect ratio (Figs. 9(e) and 13(c)). This confirms the observations of Selles [10], on PA6 90° specimens, showing undamaged *harder* cylindrical nucleii.

These observations could be explained by a phenomenon of flow-induced crystallization whereby nucleation is in part triggered by the local organisation of the polymer chains induced by the flow. Although the strain in the flow is not important enough to obtain crystallization as a shish-kebab structure [32], it might be sufficient to induce a preferential direction at the onset of crystallization. Some polymer chains extend in the molten polymer and organize themselves resulting in a cristalline structure, oriented in the flow direction, that will form the futur nucleus. Subsequent crystalline lamellae growth continues radially from this structure during cooling, thus forming an overall *spherical* arrangement around the oriented nucleus. The semi-crystalline organisation in our injection-molded thermoplastic is therefore an intermediate between purely radial spherulites and strongly oriented shish-kebab structures (Fig. 14).

This proves that the crystalline structure is not purely isotropic (contrarily to what was suggested in previous works [13]). It is also shows the necessity to better our understanding of the three-dimensional structure of spherulites in general and in our material in particular. Traditional observations on thin films and 2D description of the structure might be largely incomplete, as shown by the few deeper analysis that can be found in the literature regarding cellulose triacetate [14], poly(4-methylpentene-1) [15] and poly(oxyethylene) [33]. They describe a *rose-petal assembly* and a *square outline* of the spherulites when observed under a top plan view. These observations are consistent with the proliferation of spherulites *via* spirale growth [17]. Similar observations should be attempted on PA66 in order to complete the observations presented in this work and better describe both the spherulitic structure and the fatigue damage initiated within this structure.

Furthermore, the existing numerical models for spherulite deformation with a point-like nucleus [34,35] can be adapted to take into account the oriented nucleus structure. A model of the spherulitic damage under cyclic loading would be a major step in order to enhance current micro-mechanical models for short glass fibers composites [5,36,37].

3.3. Fractography analysis of fatigued composite specimens

In industrial applications, reinforcements are used in order to increase the mechanical performances of the material. The same type of fractography observations as presented above can thus be attempted on the composite material.

Observation of the spherulites, around 25 μm in diameter, on the fracture surface is made more difficult by the presence of the glass fibers, 10 μm in diameter. However careful examination of the fracture surface (Fig. 15(a)), in the fatigue crack path close to the notch, also allows for the observation of spherulites (Fig. 15(b) and (c)).

In particular observations on Fig. 15(d) shows the spherulites opened along a fiber, on a configuration very similar to what was observed using tomography (Fig. 7).

This confirms the scenario based on the tomographic data of fatigued composite material. Fatigue damage is closely linked to the advance of short cracks in the equatorial plane of the spherulites.

Finally, it can be noted that cavities are much more present than on the unreinforced material. This is caused by the much higher triaxiality ratios induced by the presence of glass fibers.

4. Conclusion

Traditional damage scenarios in composite materials usually include cavitation and crazing in the polymer matrix, debonding at the fiber–matrix interface and fiber failure. Tomography analyses combined with SEM fractography observations firmly establish the importance of the spherulitic arrangement of the semi-crystalline polymer. Fatigue damage progresses in the polymer by opening each spherulite in its equatorial plane, leaving one half of the spherulite to be observed on each fracture surface, with the nuclei being perfectly visible.

Observations of the nucleus also yielded a new insight on the organisation of matter in injected semi-crystalline polymers. Resulting *oriented spherulitic* structures are intermediate between the radial spherulite and the oriented shish-kebab.

Now that this scenario is confirmed, further work should evaluate the effect of different spherulite sizes and morphology on the fatigue properties and damage progress in the material.

Acknowledgement

The authors gratefully acknowledge Solvay Performance Polyamides for supporting this work and for providing specimens. Authors would also like to thank the ANRT (French National Association for Research and Technology) for its financial support via a CIFRE grant.

References

[1] Sato N, Kurauchi T, Sato S, Kamigaito O. Microfailure behaviour of randomly dispersed short fibre reinforced thermoplastic composites obtained by direct SEM observation. J Mater Sci 1991;26(14):3891–8.
[2] Horst JJ. Influence of fibre orientation on fatigue of short glassfibre reinforced Polyamide. PhD thesis, TU Delft; 1997.
[3] Nouri H, Meraghni F, Lory P. Fatigue damage model for injection-molded short glass fibre reinforced thermoplastics. Int J Fatigue 2009;31(5):934–42.
[4] Arif Muhamad Fatikul. Damage mechanisms in short glass fiber reinforced polyamide-66 under monotonic and fatigue loading: Effect of relative humidity and injection molding induced microstructure. PhD thesis, ENSAM; 2014.
[5] Rolland Héloïse. Comportement en fatigue et mécanismes d'endommagement du polyamide 6,6 renforcé de fibres courtes. PhD thesis, ENSAM; 2017.
[6] Rolland H, Saintier N, Raphael I, Lenoir N, King A, Robert G. In-situ fatigue damage mechanisms in short fibre reinforced PA66 as observed by synchrotron X-ray microtomography. Compos Part B: Eng 2018;143(December 2017):217–29.
[7] Rolland H, Saintier N, Wilson P, Merzeau J, Robert G. In situ X-ray tomography investigation on damage mechanisms in short glass fibre reinforced thermoplastics: Effects of fibre orientation and relative humidity. Compos Part B 2017;109:170–86.
[8] Arif MF, Saintier N, Meraghni F, Fitoussi J, Chemisky Y, Robert G. Multiscale fatigue damage characterization in short glass fiber reinforced polyamide-66. Compos Part B: Eng 2014;61:55–65.
[9] Galeski A, Argon AS, Cohen RE. Changes in the morphology of bulk spherulitic nylon-6 due to plastic-deformation. Macromolecules 1988;21(9):2761–70.
[10] Selles N, Cloetens P, Proudhon H, Morgeneyer T, Klinkova O, Saintier N, et al. Voiding mechanisms in deformed polyamide 6 observed at the nanometric scale. Macromolecules 2017;50(11):4372–83.
[11] Bretz PE, Hertzberg RW, Manson JA. Mechanisms of fatigue damage and fracture in semi-crystalline polymers. Polymer 1981;22(9):1272–8.
[12] E Bretz P, Manson JA, Hertzberg RW. The effect of molecular weight on fatigue crack propagation in nylon 66 and polyacetal. J Appl Polym Sci 1982;27:1707–17.
[13] Mourglia Seignobos Elodie. Compréhension des mécanismes physiques de fatigue dans le polyamide vierge et renforcé de fibres de verre. PhD thesis, INSA Lyon; 2009.
[14] Patel GN, Patel RD. Growth mechanism of polymer hedrites. Eur Polym J 1970;6(5).
[15] Khoury F, Passaglia E. The morphology of crystalline synthetic polymers. In: Hannay NB, editor. Treatise on solid state chemistry. New York: Springer; 1976. p. 335–496 [Chapter 6].
[16] Gránásy L, Pusztai T, Börzsönyi T, Tóth GI, Tegze G, Warren JA, et al. Polycrystalline patterns in far-from-equilibrium freezing: A phase field study. Phil Mag 2006;86(24):3757–78.
[17] Crist Buckley, Schultz Jerold M. Progress in polymer science polymer spherulites: a critical review. Prog Polym Sci 2016;56:1–63.
[18] King A, Reischig P, Martin S, Fonseca J, Preuss M, Ludwig W. Grain mapping by diffraction contrast tomography: extending the technique to sub-grain information.

Risø international symposium on materials science. 2010.
[19] Price Fraser P. The structure of high polymer spherulites. J Polym Sci 1959;XXXVII (April 1958):71–89.
[20] Laiarinandrasana L, Selles N, Klinkova O, Morgeneyer T, Proudhon H, Helfen L. Structural versus microstructural evolution of semi-crystalline polymers during necking under tension: Influence of the skin-core effects, the relative humidity and the strain rate. Polym Test 2016;55:297–309.
[21] Ferreiro V, Coulon G. Shear banding in strained semicrystalline polyamide 6 films as revealed by atomic force microscopy: Role of the amorphous phase. J Polym Sci, Part B: Polym Phys 2004;42(4):687–701.
[22] Detrez F, Cantournet S, Seguela R. Plasticity/damage coupling in semi-crystalline polymers prior to yielding: Micromechanisms and damage law identification. Polymer 2011;52(9):1998–2008.
[23] Zok F. Environmental fatigue crack growth in spherulitic polyethylene. J Mateilas Sci Lett 1994;3:940–3.
[24] Aboulfaraj M, G'Sell C, Ulrich B, Dahoun A. In situ observation of the plastic deformation of polypropylene spherulites under uniaxial tension and simple shear in the scanning electron microscope. Polymer 1995;36(4):731–42.
[25] Regrain C, Laiarinandrasana L, Toillon S, Saï K. Multi-mechanism models for semi-crystalline polymer: Constitutive relations and finite element implementation. Int J Plast 2009;25(7):1253–79.
[26] Ben Hadj Hamouda H, Laiarinandrasana L, Piques R. A local approach to creep fracture by slow crack growth in an MDPE: Damage modelling. Int J Press Vessels Pip 2009;86(2–3):228–38.
[27] Devilliers Clémence. Chemical degradation of PE and its influence on the creep response, damage and failure: application to lifetime assessment on pipes subjected to internal pressure. Theses, École Nationale Supérieure des Mines de Paris, December 2011, Co-encadrement de la thèse: Bruno Fayolle.
[28] Lefebvre Xavier. Fissuration fragile lente du polyamide 11: mécanismes et durées de vie en fluage. Theses, École Nationale Supérieure des Mines de Paris; December 2002.
[29] Bernasconi A, Cosmi F, Dreossi D. Local anisotropy analysis of injection moulded fibre reinforced polymer composites. Compos Sci Technol 2008;68(12):2574–81.
[30] Ayadi Abderrahmane. Modélisation et analyses expérimentales basées sur la caractérisation microstructurale par imageries a rayons X: application aux composites thermoplastiques renforcés par des fibres de verre courtes. PhD thesis, Université de Lille 1; 2016.
[31] Pantani R, Speranza V, Titomanlio G. Effect of flow-induced crystallization on the distribution of spherulite dimensions along cross section of injection molded parts. Eur Polym J 2017;97(July):220–9.
[32] Zuidema H. Flow induced crystallization of polymers application to injection moulding. PhD thesis, Technische Universiteit Eindhoven; 2000.
[33] Tien ND, Nishikawa Y, Hashimoto M, Tosaka M, Sasaki S, Sakurai S. Three-dimensional analyses of spherulite morphology in poly(oxyethylene) and its blends with amorphous poly(d,l-lactic acid) using X-ray computerized tomography. Polym J 2015;47(1):37–44.
[34] Uchida M, Tokuda T, Tada N. Finite element simulation of deformation behavior of semi-crystalline polymers with multi-spherulitic mesostructure. Int J Mech Sci 2010;52(2):158–67.
[35] Emre Oktay H, Gürses Ercan. Modeling of spherulite microstructures in semi-crystalline polymers. Mech Mater 2015;90:83–101.
[36] Klimkeit Bert. Etude experimentale et modélisation du comportement en fatigue multiaxiale d'un polymère renforcé pour application automobile. PhD thesis, ENSMA; 2009.
[37] Spahn Johannes. An Efficient Multiscale Method for Modeling Progressive Damage in Composite Materials. PhD thesis, TU Kaiserslautern; 2015.